# Hot-Wire Anemometer Based on D-Shaped Optical Fiber

Elena De Vita, *Member, IEEE*, Pasquale Di Palma, Sidrish Zahra, Giuseppina Roviello, Claudio Ferone, Agostino Iadicicco, *Member, IEEE*, and Stefania Campopiano, *Member, IEEE*

***Abstract*—This article proposes a hot-wire anemometer based on optical fiber embedding a fiber Bragg grating (FBG) and having a D-shaped transversal section on whose flat surface a thin metallic layer has been deposited. Due to this geometrical structure, the optical power flowing through the fiber core can achieve the metallic layer and can be converted into heat. The embedded FBG can measure the resulting temperature increase and the temperature fluctuation of the D-fiber caused by the wind flowing. Numerical simulations have been performed in order to select the appropriate design parameters, such as thickness of the metallic layer and its distance from the core. Then, the fabrication process of the device and the experimental results of its characterization in temperature and wind assess its working principle. The developed sensor can work at low power levels of the source and is characterized by small size and high accuracy. Furthermore, it shows high cost-effectiveness and the possibility to modulate its wind sensitivity by setting the source power.**

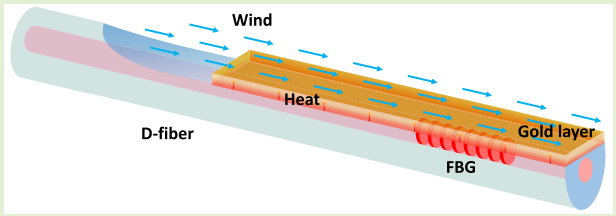


***Index Terms*— D-fiber, fiber Bragg gratings (FBGs), fiber-optic anemometer, hot-wire anemometer (HWA), thermoplasmonic effect.**

## I. Introduction

MEASUREMENTS of fluid flow with high accuracy have received a great deal of attention due to their significant uses in the aerospace industry, chemical engineering, and energy. The development of flow sensors has been demonstrated using several methods, such as measuring the duration of flight [1], measuring differential pressure [2], and measuring heat transfer [3], [4]. However, currently, it is exceedingly expensive and difficult to install a significant number of flow sensors. Recently, optical fiber-based flow sensors have received a lot of attention among research and industry applications due to their intrinsic characteristics, such as electrically passive operation, long lifetime, and immunity to electromagnetic interference.

Manuscript received 24 March 2023; revised 14 April 2023; accepted 14 April 2023. Date of publication 27 April 2023; date of current version 14 June 2023. This work was supported by the Ministero dell'Istruzione e del Merito–Programma Operativo Nazionale (MIUR-PON) "Research & Innovation"/PNR 2015-2020 within the Framework of "Nanophotonics for New Diagnostic and Therapeutics Approaches in Oncology and Neurology NeON" under Grant ARS01_00769 CUP B26C18000110005. The associate editor coordinating the review of this article and approving it for publication was Prof. Carlos Marques. *(Corresponding author: Pasquale Di Palma.)*

The authors are with the Department of Engineering, University of Naples Parthenope, 80143 Naples, Italy (e-mail: elena.devita@collaboratore.uniparthenope.it; pasquale.dipalma@collaboratore.uniparthenope.it; sidrish.zahra001@studenti.uniparthenope.it; giuseppina.roviello@uniparthenope.it; claudio.ferone@uniparthenope.it; agostino.iadicicco@uniparthenope.it; stefania.campopiano@uniparthenope.it).

Digital Object Identifier 10.1109/JSEN.2023.3269661

To date, various optical fiber anemometers have been reported [5], [6], [7], [8], [9], [10], [11], [12], [13], [14], [15], [16], [17], [18], [19], [20]. Most of these are based on the photothermal effect, where heat is generated through a light source and airflow will lower the temperature of the fiber-optic element. The experimental setup of these hot-wire anemometers (HWAs) usually includes a high-power pump laser (hundreds of milliwatts), an optical coupling structure, and a metal-coated fiber generating the heat.

Previously, various core-to-cladding coupling structures were used to carry the light out of the core and heat the external layers, including the fiber Bragg grating (FBG) structure, long-period grating (LPG), multimode fiber (MMF) and single-mode fiber (SMF) splicing, core offset, and bitaper [5], [6], [8], [9]. Few shortcomings are related, for example, to the bending sensitivity of MMF and LPG, which makes it difficult to maintain a constant coupling coefficient in practice. Moreover, the mechanical strength of the fiber used in the core-offset fusion splice method is relatively low, making it difficult to measure high-velocity airflow.

In 2012, a compact anemometer was proposed in [5], which is based on an FBG coated with a silver film of 120 nm thickness and assisted by a core-offset fusion splice causing a heating effect of approximately 56 °C at the maximum input power of 450 mW. Successfully, the same authors confirmed increased mechanical strength and more stable coupling efficiency (approximately 90%) using a silver-coated

FBG assisted by a waist-enlarged fiber bitaper. The airflow velocity measurement achieved a high sensitivity of 47.2 pm/(m/s) [6].

Even though metal-coated fiber performs well, different studies have also focused on different kinds of materials to improve optical power absorption and thermal conductivity. Tilted FBG has been successfully used in fiber-optic HWA when combined with a single-walled carbon nanotubes (SWCNTs) coating. Despite achieving a high-efficiency and compact all-optical fiber HWA, this scheme lacks stability and results in a lower signal-to-noise ratio in the resonance spectrum [8]. Liu et al. [7] utilized a carbon nanotube coating-based tilted FBG-assisted surface plasmon resonance and found that when the sensor was heated with a total power of 10 mW, the actuation efficiency of about 2.2 °C/mW can be achieved.

Caldas et al. [9] proposed a novel lossless process to increase the temperature of the thin silver film by light coupling using an LPG as a coupling element to terminate the limitation of the SM/MM fiber-based strategy concerning substantial losses due to mismatching characteristics of the two fibers.

It is also worth mentioning the approach recently proposed in [10], regarding the thermoplasmonic effects achieved onto a gold nanostructure made of a periodic array of nanoholes directly integrated on the optical fiber tip. Liu et al. [11] proposed a fiber-optic microheater based on a miniature Fabry–Pèrot interferometer, which was spliced to the end face of SMF: this microheater has temperature self-gauging capability with operation temperature above 1000 °C. Although it has high-temperature capability, it requires specialized and expensive components, which increases the cost of the device ultimately. Very recently, Zhang et al. [15] reported an intensity-interrogated optical fiber thermal anemometer based on the chirp effect of FBG coated with silver film that achieved a high sensitivity of 28.60 W/(m/s).

To observe the Bragg wavelength shift of FBG in the aforementioned HWA, a broadband light source is required, and to heat up these hot wires, a pump laser with a power of several hundred milliwatts is required, making the sensing system relatively complex and expensive.

In this article, we propose an anemometer consisting of a simple structure, i.e., D-shaped optical fiber, where a high-power laser pump is not required to heat up hot wire. D-shaped fiber-optic structures offer several advantages such as easy deposition process and more robustness with respect to uncladded and tapered configurations [21]. In our tests, a broadband light source also serves as a heating light source, obviating the need for a heating resistor or a pump laser.

## II. Sensor Structure and Principle

The proposed anemometer is based on an etched fiber with a resulting D-shape covered by a thin gold layer, as shown in Fig. 1.

The considered values of gold layer thickness, denoted by $S$, and cladding thickness between core and gold layer, denoted by $D$, and their combinations are reported in Table I.

By removing a portion of cladding (lengthwise) of the optical fiber approximately until the core of the fiber, the evanescent wave from the core of the fiber will strongly interact with the external medium, i.e., it will be gradually absorbed by the metal layer deposited on the flat surface of the D-shape fiber, with the power decreasing exponentially along the distance. It can be stated that the optical power $P$ will decrease according to the following equation [15]:

$$P(z) = P_{\text{input}} \cdot \varphi \cdot e^{-\alpha_m \cdot z} \tag{1}$$

where $P_{\text{input}}$ is the input power of the optical source, $\varphi$ is the coupling coefficient of D-fiber, $\alpha_m$ is the absorption coefficient of the metal film, and $z$ is the distance starting from the enter side of the metal film.

In order to evaluate the proper thicknesses $S$ and $D$, simulations are performed in the COMSOL Multiphysics[1] environment (version 5.1) by considering the values reported in Table I, and the parameters of a standard SMF28 are used for the refractive indices and core diameter.

The simulated electric field distribution in the central region of the gold-coated D-fiber is reported for each value of $D$ and $S$ in Fig. 2. As it can be seen, in order to have a significant electric field from the core to the metal layer, a cladding thickness $D$ as thin as 1 $\mu$m is needed and, for the simulated values of $D$ and $S$, the highest field in the metal layer is obtained for $D = 0.1$ $\mu$m and $S = 1$ $\mu$m.

Thus, with a thin cladding layer between the core and the metal, the metal film absorbs the source light and converts it into heat, which raises the temperature of the D-fiber. This effect can be used to realize an optical fiber HWA. Indeed, when the airflow blows, the heat loss accelerates, which in turn lowers the temperature of the D-fiber until a new thermal equilibrium is reached. The following relationship for the heat loss $H_{\text{Loss}}$ can be achieved, if the temperature at a certain point of the D-fiber under airflow at velocity $v$ is $T_V$ [16], [17]:

$$H_{\text{Loss}} = [T_V - T_a] \cdot \left(A + B \cdot v^n\right) \tag{2}$$

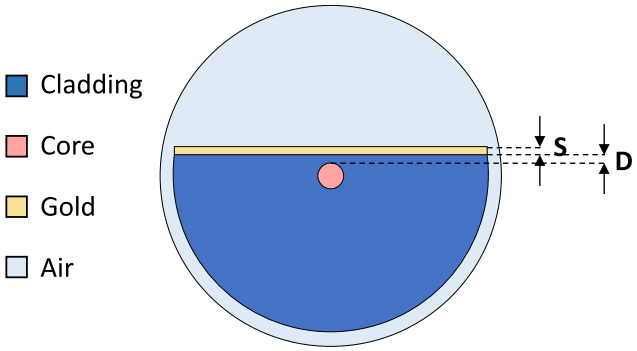


Fig. 1. Schematic of the transversal section of the D-Fiber coated with a thin gold layer (not to scale).

TABLE I
Values of $S$ and $D$

| $D$ [μm] | $S$ [μm] | | |
|---|---|---|---|
| 0.1 | 0 | 0.05 | 1 |
| 1 | 0 | 0.05 | 1 |
| 5 | 0 | 0.05 | 1 |

[1]Registered trademark.

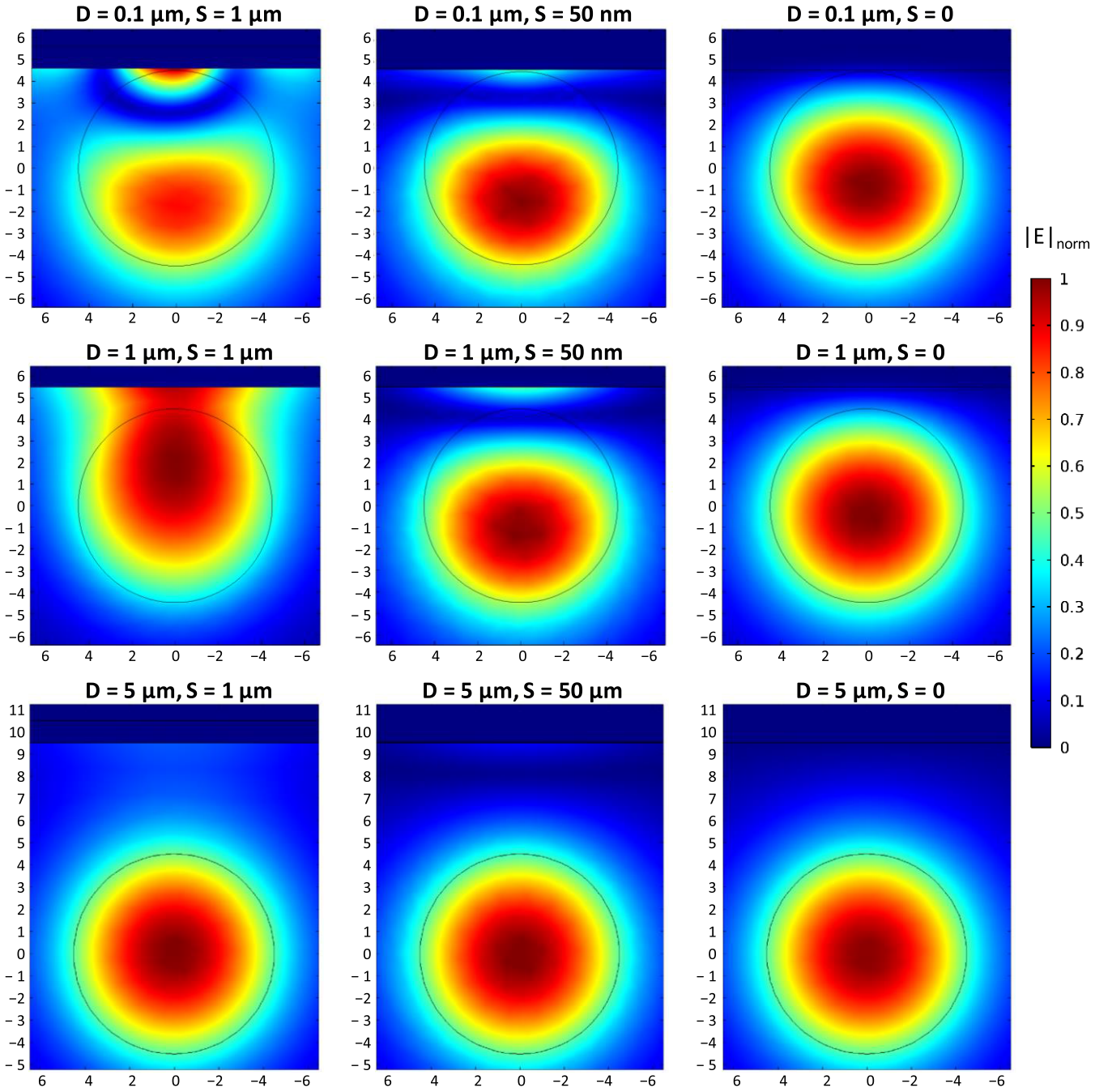


Fig. 2. Normalized electric field for different values of $D$ and $S$.

where $T_a$ is the airflow temperature and $A$, $B$, and $n$ are empirical coefficients.

Assuming that heat generation and loss are in equilibrium, the following relationship can be obtained [17]:

$$H_{\text{Loss}} = P\,(z) \cdot \alpha_m \cdot \beta \tag{3}$$

where $\beta$ is the converting coefficient of the absorbed optical power to heat by the metal film and $\alpha_m$ is the absorption coefficient of the metal film.

If an FBG is inscribed along the anemometer as can be seen in Fig. 3, then the Bragg wavelength of the FBG changing with temperature of the anemometer $\lambda$ can be described as

$$\lambda - \lambda_o = K \cdot (T_V - T_a) \cdot \lambda_o \tag{4}$$

where $K$ is the temperature coefficient of sensitivity of D-fiber and $\lambda_o$ is the Bragg wavelength without heating. The relationship between the Bragg wavelength of the FBG and the airflow velocity can thus be expressed as

$$\lambda = \lambda_o \cdot \left(1 + \frac{K \cdot P\,(z) \cdot \alpha_m \cdot \beta}{(A + B \cdot v^n)}\right). \tag{5}$$

Based on this equation, the airflow velocity can be determined from the measured wavelength shift of the FBG.

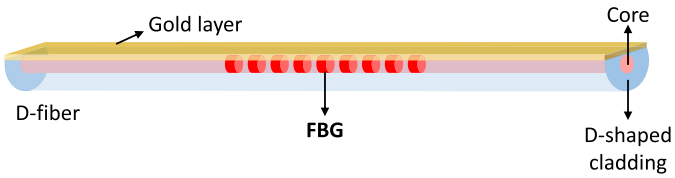


Fig. 3. Schematic of the gold-coated D-fiber embedding an FBG.

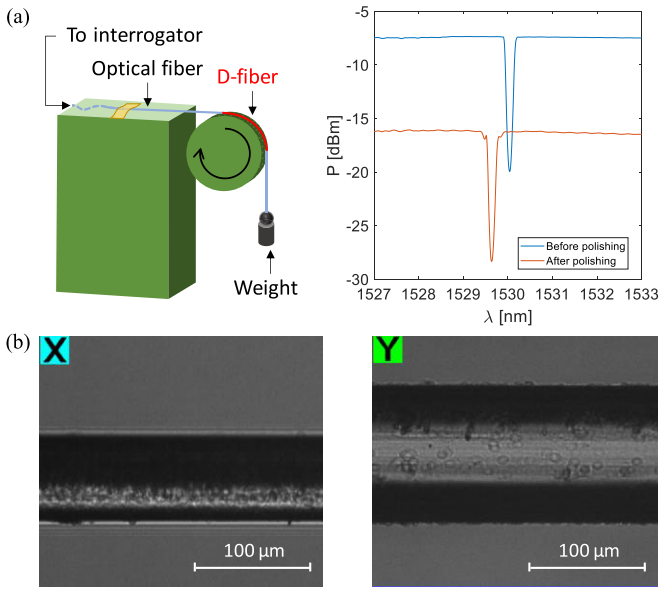


Fig. 4. (a) Setup for fabricating the D-fiber (on the left) and optical transmitted spectrum of the FBG before and after the polishing procedure for the D-shaping (on the right). (b) Microscope images from orthogonal views of the D-fiber made with the illustrated setup.

## III. Sensor Fabrication

The D-fiber is manufactured by using single-mode glass optical fiber (SMF28) with a core diameter of 8 $\mu$m and a cladding diameter of 125 $\mu$m and embedding a 10-mm-long commercial FBG produced by AtGrating Technologies. An extremely fine grain polishing abrasive wheel is part of the setup for creating the D-section fiber, which is shown in the left of Fig. 4(a). The wheel is powered by a low-speed electric motor and has a diameter of 76 mm, and the optical fiber region affected by the processing has a diameter of about 60 mm. As shown in Fig. 4, the optical fiber that needs to be shaped is blocked on one side, set on the abrasive wheel, and then tensioned by placing a weight of 14 g on the opposite side of the fiber. On the right, Fig. 4(a) shows the optical spectrum transmitted by the FBG before (blue curve) and after (red curve) the polishing performed to achieve the D-shaped fiber section. As can be noted, at the end of the polishing, the spectrum transmitted by the FBG results shifted down and the wavelength peak shifted to the left. The downward shift is the index of successful polishing since it is due to the decrease of the power transmitted by the grating caused by the thinning of cladding. At the same time, a left shift of the FBG peak occurs because of the decrease of the effective refractive index of the core mode due to the cladding thinning, also in accordance with COMSOL simulations.

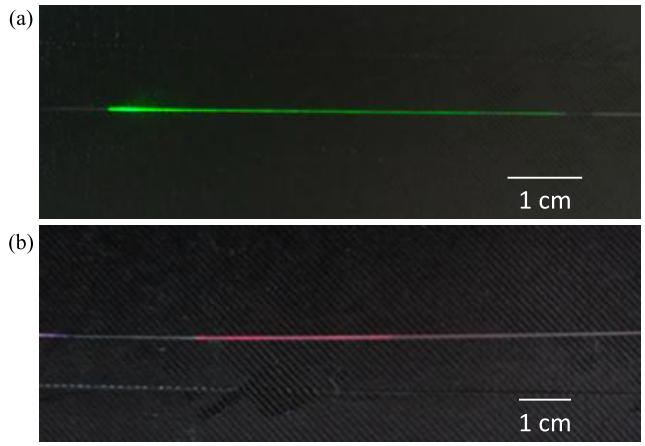


Fig. 5. Photograph of the D-fiber excited with laser lights in (a) green region, i.e., at a wavelength of 532 nm, and (b) red region, i.e., at a wavelength of 650 nm.

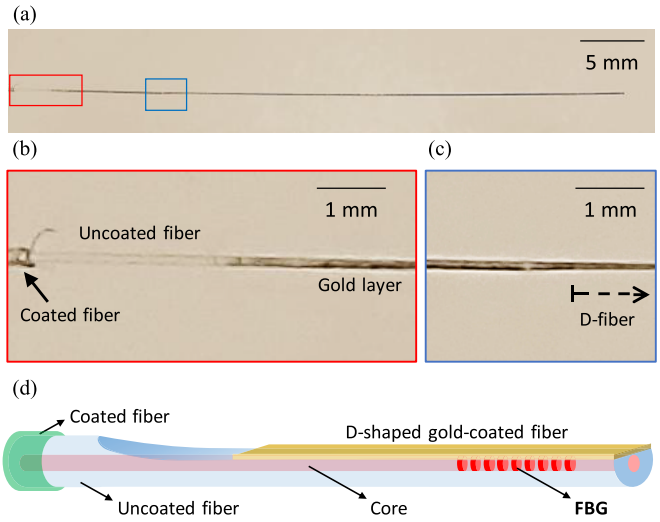


Fig. 6. (a) Side view of the fabricated device, magnified in correspondence of (b) the red rectangle to show the acrylate coating and the gold layer deposited on the uncoated fiber and (c) the blue rectangle to show the beginning of D-fiber region. (d) Schematic of the fiber after D-shaping and gold layer deposition.

Fig. 4(b) shows two microscope images at two orthogonal views of the D-fiber section in the machined region, labeled X and Y. As can be seen, the X-view shows a much thinner fiber profile than the one from the Y-view, demonstrating the effectiveness of the employed manufacturing process of D-shaping.

Once the fiber is thinned, green (532 nm) and red (650 nm) laser lights are launched in the fiber as can be seen in Fig. 5(a) and (b), respectively, where it is possible to see the evanescent field irradiating from the core.

The next step is the deposition of a thin gold layer by means of a sputter coater (Q150RS by Quorum Technologies). Gold metal has been selected because of its high chemical resistance to oxidation.

In Fig. 6(a), the photograph with a magnifying glass of the final device is reported, whereas, in Fig. 6(b) and (c), the zoom of the blue and the red rectangles in Fig. 6(a) is reported, respectively.

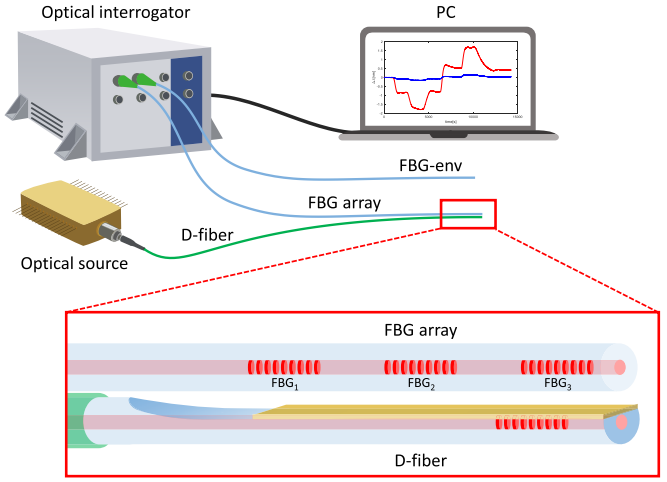


Fig. 7. Experimental setup implemented for the thermal characterization.

In particular, Fig. 6(b) shows the zoom in correspondence of the first part of the etched fiber (indeed, it is possible to see a zone without metal layer), whereas in Fig. 6(c), the zoom in a more central region is reported, showing the initial portion of the D-fiber.

## IV. Experimental Results and Discussion

In this section, the temperature and wind characterizations of the developed device are reported and discussed, and the experimental setup employed during the tests is described.

### A. Thermal Characterization

For the thermal characterization of the anemometer, the experimental setup shown in Fig. 7 is used, involving the following components:

1) optical source: superluminescent light emitting diode (SLED Exalos 1550 nm);
2) FBG array with three FBGs for temperature measurements;
3) an FBG for measuring the environmental temperature (FBG-env);
4) optical interrogator (HBM FS22 BraggMeter);
5) PC.

The light from a broadband optical source is injected into the D-fiber to induce the heating effect in the overlying gold layer. To measure such heating, an external array consisting of three FBGs each one 3 mm long is placed along the D-fiber as close as possible to the metallic surface. The array measurements are recorded by the optical interrogation system in the wavelength range from 1500 to 1600 nm and displayed by means of a PC connected to the interrogator.

When the broadband source is turned on and enters the D-fiber, due to the thin cladding layer, the evanescent field from the core couples with the gold layer, which in turn absorbs it causing the heating effect. The heat generated due to radiation absorption induces a temperature increase in the D-fiber region, which can be detected by the array of FBGs. As reported in Fig. 8, temperature variation is proportional

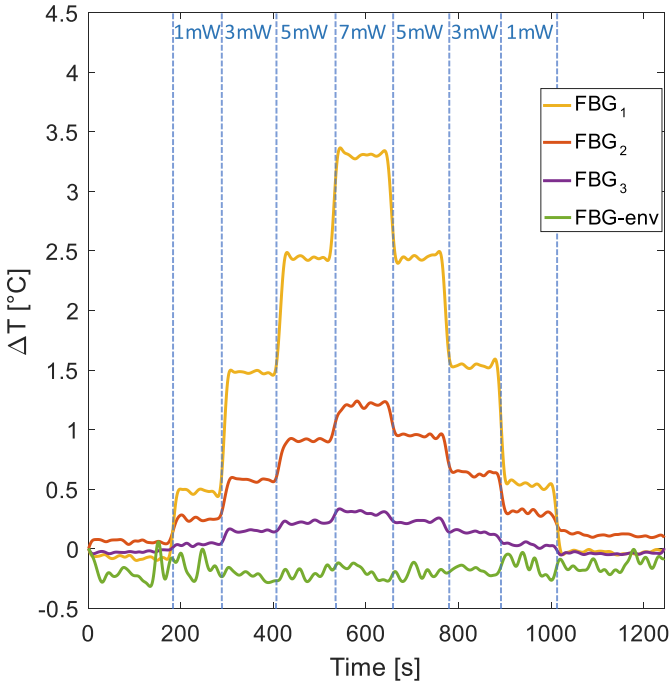


Fig. 8. Trends of temperature variation $\Delta T$ recorded by the array and FBG-env as a function of time.

to the power of the broadband source: when the power is increased from 0 to 1 mW and is kept stable for 10 s, the heating effect starts to increase. As a result, the temperature continues to increase until power is increased to 7 mW, especially for the FBGs closest to the initial portion of the D-fiber, i.e., $FBG_1$ and $FBG_2$, as can be inferred from the yellow and red profiles in Fig. 8, respectively. The maximum rise in temperature was observed when the power of the broadband source is 7 mW, and a decreasing trend of temperature can be observed as the power of the broadband source is gradually reduced.

### B. Wind Characterization

To test the capability of the developed device to detect the wind changes, the experimental setup shown in Fig. 9 is used. It is made up of the following components:

1) optical source: superluminescent light emitting diode (SLED Exalos 1550 nm);
2) fiber-optic circulator;
3) wind tunnel;
4) two FBGs for temperature measurements;
5) optical spectrum analyzer (OSA-AQ6370B);
6) optical interrogator (HBM FS22 BraggMeter);
7) PC.

The optical source, set to 7 mW, is used to generate heat in the D-fiber through absorption of the gold layer and simultaneously to illuminate the inner FBG, denoted by FBG-D, for interrogation. To read the data from FBG-D, it has been connected to Port 2 of the fiber-optic circulator together with the SLED (Port 1) and the OSA recording the spectra (Port 3). The D-fiber has been located inside a custom miniaturized wind tunnel together with two other FBGs, i.e., FBG-ext and

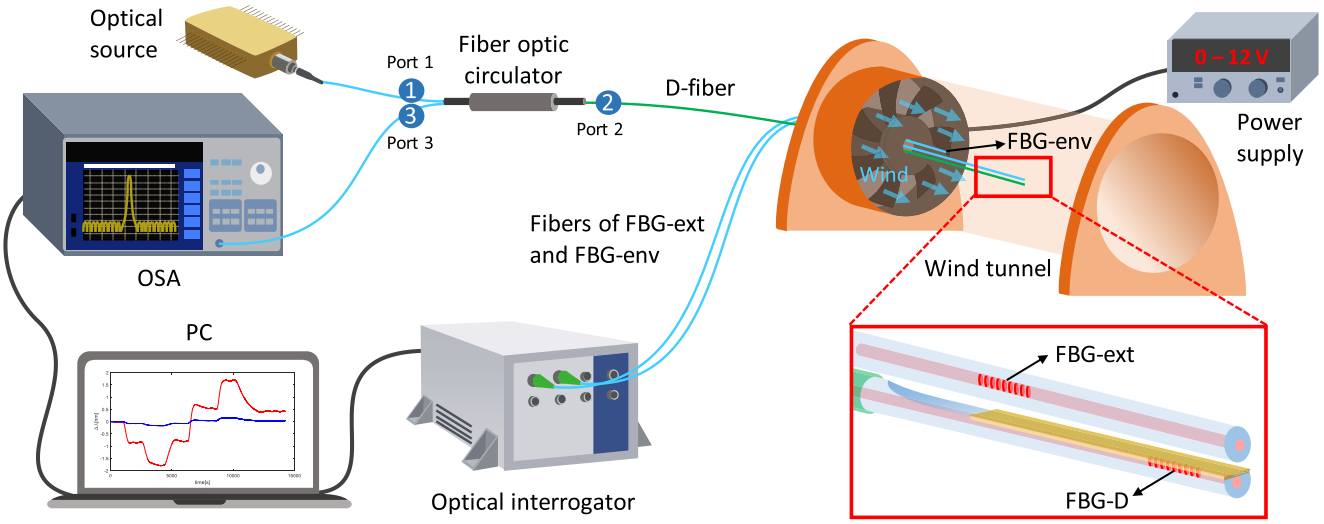


Fig. 9. Schematic of the proposed experimental setup implemented for the wind characterization.

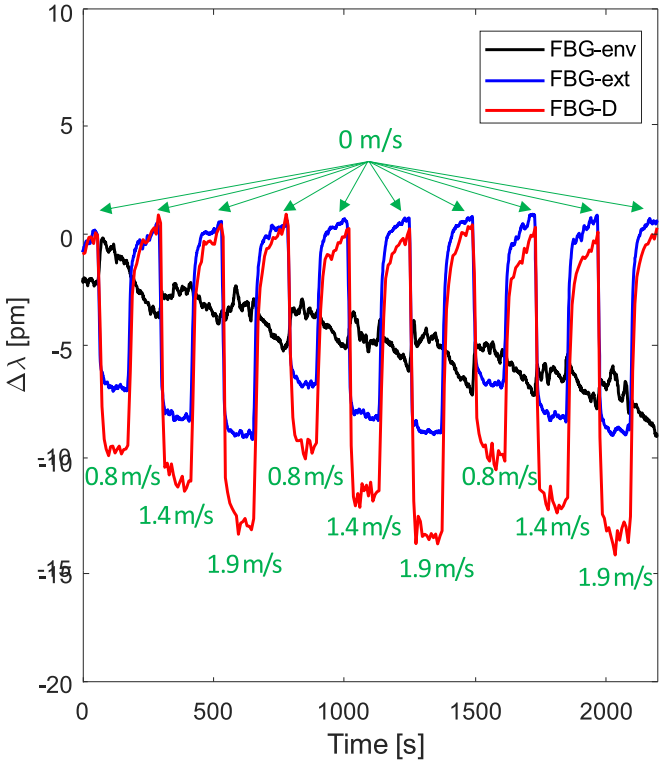


Fig. 10. Wavelength variations as a function of time recorded by FBG-D (red line), FBG-ext (blue line), and FBG-env (black line).

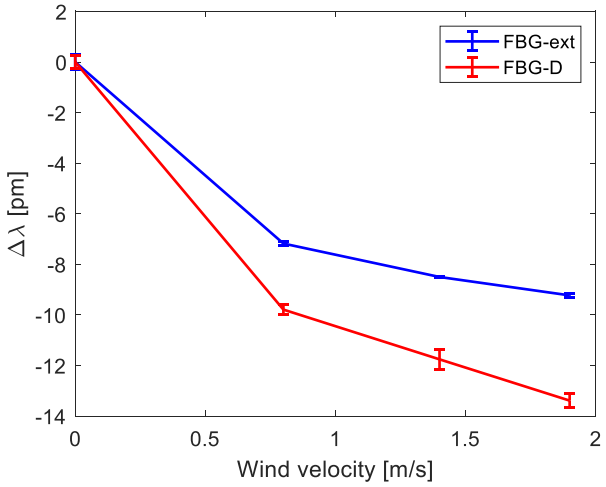


Fig. 11. Wavelength variations as a function of time recorded by FBG-D (red line), FBG-ext (blue line), and FBG-env (black line). Results of the wind characterization recorded by FBG-D and FBG-ext.

FBG-env. The wind tunnel consists in: 1) a miniaturized tube 12 cm in diameter and 40 cm long; 2) a small fan fixed at one end; and 3) a power supply to power the fan and set the wind velocity. FBG-D is positioned at the center of the wind tunnel and measures the wind variations from inside the D-fiber; FBG-ext is placed on the D-fiber in correspondence of the beginning of the etched region to provide measurements from outside the D-fiber in a different point with respect to FBG-D; FBG-env is located in the tunnel to measure the air temperature.

Both FBG-ext and FBG-env are connected to the optical interrogator, which collects their wavelength values, obtained by means of an algorithm based on the baricentral calculation, with a resolution of 1 pm and a sampling frequency of 1 sample/s. The measured data are displayed and recorded by a PC connected to the optical interrogator.

The wind tests are performed at three velocities, i.e., 0.8, 1.4, and 1.9 m/s, by setting the power supply accordingly, measuring such values by means of a reference digital anemometer (Proster TL017) with a resolution of 0.1 m/s.

Several experimental tests have been carried out, and a set of them are shown in Fig. 10.

During each test, before each variation of wind velocity, the fan is set at 0 m/s. In particular, in Fig. 10, three reiterated tests are reported, displaying the temporal trends of the wavelength variations (i.e., $\Delta\lambda$) recorded by the three FBGs. FBG-env measures only the tunnel temperature trend during the tests (black profile). The $\Delta\lambda$ profiles of FBG-D and FBG-ext (red and blue profiles, respectively) are reported

after the temperature compensation operation, showing that increasing wind velocities induce $\Delta\lambda$ decreases because of the temperature decrease in the device.

The results of the wind characterization recorded by FBG-D and FBG-ext are shown in Fig. 11, showing a nonlinear relationship with the airflow velocity. This phenomenon could be due to the limited heating of the D-fiber. Indeed, the temperature decrease due to the wind flux cannot exceed the temperature increasing inside the D-fiber caused by the gold layer absorption. The nonlinear behavior is common to the HWAs [15]. Furthermore, as expected, FBG-ext exhibits a lower wind sensitivity with respect to FBG-D since it is located outside the D-fiber just leaning on it and, thus, only partially in contact with the D-fiber.

## V. Conclusion

This article reports about the concept and development of an HWA based on a single-mode optical fiber. The temperature increment is enabled by the particular structure implemented on the fiber connected to a power light source. Indeed, the D-shaped transversal section of the fiber allows the power extraction from the core and the gold layer deposited on the flat surface converts the optical power to heat, inducing the temperature increase of D-fiber.

To measure the temperature variations due to the wind flowing on the metallic surface, an FBG embedded inside the D-fiber is exploited.

The developed sensor exhibits small size, high cost-effectiveness, and high accuracy. The device can work at low power levels of the source (7 mW in this case). It is worth noting that, by increasing the source power, the gold layer can achieve higher temperature variations, and thus, the wind sensitivity of the device can be enhanced.

Future developments will involve the implementation of embedding strategies to strengthen the D-fiber structure and improve its handling by encapsulating the optical fiber in 3-D printed packages before the polishing procedure [22], [23]. Moreover, the exploited working principle can be extended to different kinds of optical fibers, such as polymer fibers to enhance the device robustness.

## References


[1] J. Wu and W. Sansen, "Electrochemical time of flight flow sensor," *Sens. Actuators A, Phys.*, vols. 97–98, pp. 68–74, Apr. 2002.

[2] N. Svedin, E. Kalvesten, and G. Stemme, "A new edge-detected lift force flow sensor," *J. Microelectromech. Syst.*, vol. 12, no. 3, pp. 344–354, Jun. 2003.

[3] S. Oda, M. Anzai, S. Uematsu, and K. Watanabe, "A silicon micromachined flow sensor using thermopiles for heat transfer measurements," *IEEE Trans. Instrum. Meas.*, vol. 52, no. 4, pp. 1155–1159, Aug. 2003.

[4] M. Dominguez et al., "Low-cost thermal $\Sigma - \Delta$ air flow sensor," *IEEE Sensors J.*, vol. 2, no. 5, pp. 453–462, Oct. 2002.

[5] X. Dong, Y. Zhou, W. Zhou, J. Cheng, and Z. Su, "Compact anemometer using silver-coated fiber Bragg grating," *IEEE Photon. J.*, vol. 4, no. 5, pp. 1381–1386, Oct. 2012.

[6] X. Wang, X. Dong, Y. Zhou, Y. Li, J. Cheng, and Z. Chen, "Optical fiber anemometer using silver-coated fiber Bragg grating and bitaper," *Sens. Actuators A, Phys.*, vol. 214, pp. 230–233, Aug. 2014.

[7] Y. Liu et al., "Plasmonic fiber-optic photothermal anemometers with carbon nanotube coatings," *J. Lightw. Technol.*, vol. 37, no. 13, pp. 3373–3380, Jul. 1, 2019.

[8] Y. Zhang et al., "Fiber-optic anemometer based on single-walled carbon nanotube coated tilted fiber Bragg grating," *Opt. Exp.*, vol. 25, no. 20, Oct. 2017, Art. no. 24521.

[9] P. Caldas et al., "Fibre optic hot-wire flowmeter based on a metallic coated hybrid LPG-FBG structure," *Proc. SPIE*, vol. 7653, Sep. 2010, Art. no. 76530B, doi: 10.1117/12.866463.

[10] S. Principe et al., "Thermo-plasmonic lab-on-fiber optrodes," *Opt. Laser Technol.*, vol. 132, Dec. 2020, Art. no. 106502.

[11] G. Liu, Q. Sheng, D. Dam, J. Hua, W. Hou, and M. Han, "Self-gauged fiber-optic micro-heater with an operation temperature above 1000 °C," *Opt. Lett.*, vol. 42, no. 7, p. 1412, Apr. 2017.

[12] G. M. Berruti et al., "Highly efficient fiber optic thermal heating device based on turn-around-point long period gratings," *J. Lightw. Technol.*, vol. 40, no. 3, pp. 797–804, Feb. 1, 2022.

[13] D. Hu et al., "Plasmonic gold nanostar mediated self-photothermal modulation of microfiber Bragg grating," *J. Lightw. Technol.*, vol. 40, no. 14, pp. 4812–4818, Jul. 15, 2022.

[14] J. Zhang, X. Dong, P. Xu, D. Lv, J. Yang, and Y. Qin, "Optical fiber thermal anemometer with light source-heated Fabry–Pérot interferometer," *J. Lightw. Technol.*, vol. 40, no. 9, pp. 3010–3015, May 1, 2022.

[15] J. Zhang, Y. Tang, P. Xu, O. Xu, and X. Dong, "Intensity-interrogated hot-wire anemometer based on chirp effect of a fiber Bragg grating," *Opt. Exp.*, vol. 30, no. 20, Sep. 2022, Art. no. 37124.

[16] J. Wang, Z.-Y. Liu, S. Gao, A. P. Zhang, Y.-H. Shen, and H.-Y. Tam, "Fiber-optic anemometer based on Bragg grating inscribed in metal-filled microstructured optical fiber," *J. Lightw. Technol.*, vol. 34, no. 21, pp. 4884–4889, Nov. 1, 2016.

[17] S. Gao, A. P. Zhang, H.-Y. Tam, L. H. Cho, and C. Lu, "All-optical fiber anemometer based on laser heated fiber Bragg gratings," *Opt. Exp.*, vol. 19, no. 11, May 2011, Art. no. 10124.

[18] G. E. W. Hartley, "The development of electrical anemometers," *Proc. IEE II, Power Eng.*, vol. 98, no. 64, pp. 430–437, Aug. 1951.

[19] H. H. Bruun, "Hot-wire anemometry: Principles and signal analysis," *Meas. Sci. Technol.*, vol. 7, no. 10, p. 24, Oct. 1996.

[20] F. Wang et al., "Fiber-optic hot-wire anemometer with directional response based on symmetry-breaking induced heat transfer mechanism," *J. Lightw. Technol.*, vol. 39, no. 12, pp. 3919–3925, Jun. 15, 2021.

[21] M. S. Soares et al., "Label-free plasmonic immunosensor for cortisol detection in a D-shaped optical fiber," *Biomed. Opt. Exp.*, vol. 13, no. 6, p. 3259, Jun. 2022.

[22] P. Di Palma, E. De Vita, A. Iadicicco, and S. Campopiano, "3D shape sensing with FBG-based patch: From the idea to the device," *IEEE Sensors J.*, vol. 22, no. 2, pp. 1338–1345, Jan. 2022.

[23] P. Di Palma, E. De Vita, A. Iadicicco, and S. Campopiano, "Force sensor based on FBG embedded in silicone rubber," *IEEE Sensors J.*, vol. 23, no. 2, pp. 1172–1178, Jan. 2023.



**Elena De Vita** (Member, IEEE) received the M.Sc. (cum laude) degree in biomedical engineering from the Università Campus Bio-Medico di Rome, Rome, Italy, in 2018, and the Ph.D. degree in information and communication technology and engineering from the University of Naples Parthenope, Naples, Italy, in 2022.

She is currently a Postdoctoral Researcher with the Department of Engineering, University of Naples Parthenope. Her current research interests include fiber-optic sensors in biomedical and industrial applications for thermal and mechanical measurements.

**Pasquale Di Palma** received the M.Sc. degree in telecommunications engineering from the University of Naples Federico II, Naples, Italy, in 2015, and the Ph.D. degree in information engineering from the University of Naples Parthenope, Naples, in 2019.

Since 2015, he has been with the Department of Engineering, University of Naples Parthenope. His current research interests include the design, simulation, fabrication, and characterization of fiber-optic sensors for physical, chemical, and biological applications.

**Sidrish Zahra** received the master's degree in information and communication engineering from the University of Electronic Science and Technology of China, Chengdu, China, in 2019. She is currently pursuing the Ph.D. degree in information and communication technology and engineering with the University of Naples Parthenope, Naples, Italy.

Her current research interests include the fabrication and characterization of optical fiber sensors for optical fiber communication and sensing applications.

**Giuseppina Roviello** received the master's (cum laude) degree in chemistry and the Ph.D. degree in chemical science from the University of Naples Federico II, Naples, Italy, in 2000 and 2003, respectively.

She is currently an Associate Professor of Chemical Foundations of Technologies at the Department of Engineering, University of Naples Parthenope, Naples. Her scientific personality presents a wide range of interests, which involve the area of coordination chemistry and span from investigation of fundamental reaction mechanisms to the development of new strategic synthesis of materials for innovative application fields, e.g., optoelectronics or asymmetric catalysis. Her current research activity concerns the synthesis and study of the structure–property relationship of new inorganic and organic–inorganic hybrid materials obtained from the valorization of secondary raw materials for applications in the sustainable civil engineering and environmental remediation field.

**Claudio Ferone** received the master's (cum laude) degree in chemical engineering and the Ph.D. degree from the University of Naples Federico II, Naples, Italy, in 1995 and 1998, respectively.

He is currently an Associate Professor of Chemical Foundations of Technology at the Department of Engineering, University of Naples Parthenope, Naples. His scientific work resulted in 105 indexed publications in international journals and conference proceedings, with an H-index of 35, and he has coauthored patents. The scientific research has focused mainly on the study of natural and artificial inorganic materials for applications in various areas, such as materials for civil engineering and advanced ceramics. Currently, he is concerned with the treatment and valorization of natural and industrial wastes through innovative, low environmental impact, processes.

Dr. Ferone is a member of the Ph.D. Teaching Council in Energy Science and Engineering. He is a Chief Editor of the specialty section Alternative Materials of the *Frontiers in Sustainability* journal and is a member of the Editorial Board of the *Materials* and *Environments* journals, edited by MDPI, and *SN Applied Sciences* (Springer Nature).

**Agostino Iadicicco** (Member, IEEE) received the master's (cum laude) degree in electronic engineering from the Second University of Naples, Naples, Italy, in 2002, and the Ph.D. degree in information engineering from the University of Sannio, Benevento, Italy, in 2005.

He is currently a Professor with the Department of Engineering, University of Naples Parthenope, Naples. Since 2002, his research activity has been focused on optoelectronics and photonics devices for sensing and communications applications. He is currently involved in the design, realization, and testing of novel in-fiber devices in standard and unconventional fibers, including polarization-maintaining and photonic bandgap fibers. His work in this area encompasses the development and practical application of sensors for the measurement of a range of physical, chemical, and biological parameters.

Dr. Iadicicco is a member of the Ph.D. Teaching Council and serves as an Associate Editor for the IEEE SENSORS JOURNAL.

**Stefania Campopiano** (Member, IEEE) received the master's (cum laude) degree in electronic engineering from the University of Naples Federico II, Naples, Italy, and the Ph.D. degree in electronic engineering from the Università della Campania L. Vanvitelli, Caserta, Italy.

She is currently a Full Professor of Electronics and Optoelectronics with the University of Naples Parthenope, Naples. She is also a Ph.D. Teaching Staff Member. She is a Tutor of several Ph.D. students. Her main research field is in the area of optoelectronic sensors and devices. She has authored over 200 printed works, including international journals and conferences, and coauthored patents. She cooperates on scientific arguments with several universities and companies in Italy and abroad. Her current research interests include nondestructive characterization of semiconductor and dielectric materials, integrated optic sensors, and fiber-optic and fiber Bragg grating (FBG)-based sensors systems.

Dr. Campopiano is the pro-tempore Chair of the Italy Chapter of the IEEE Sensor Council.